J. Fluid Mech. (2010), *vol.* 647, *pp.* 143–161. © Cambridge University Press 2010
doi:10.1017/S0022112009993077

Marangoni effects caused by contaminants adsorbed on bubble surfaces

PETER LAKSHMANAN AND PETER EHRHARD†

Fluid Mechanics, Biochemical & Chemical Engineering, Technische Universität Dortmund, Emil-Figge-Strasse 68, D-44221 Dortmund, Germany

(Received 4 August 2009; revised 26 October 2009; accepted 26 October 2009)

The influence of Marangoni stresses, caused by contaminants adsorbed on the surface of small air bubbles, rising in water, is examined by numerical simulations. A modified level set method is used to represent the deformable bubble interface, extended by a model for the contaminant transport on the bubble surface. We show that surface tension variations of less than 2 % are sufficient to generate Marangoni stresses that are strong enough to change the rising characteristics of a bubble to that of a corresponding solid particle. In such situations, we find that the bubble surface is fully covered with contaminant and the shear stress profile resembles the shear stress profile around a solid sphere.

1. Introduction

Dispersed gas bubbles play an important role in many industrial applications. Distillation, extraction and heterogeneous catalysis are only a few among a multitude of applications. The bubble size distribution, the breakup and coalescence behaviour and the velocity relative to the surrounding liquid determine the interfacial area and the residence time, the two most important parameters for heat and mass transfer. Therefore, understanding the bubble behaviour appears crucial for process design. Hence, knowing the fundamental behaviour of single bubbles is mandatory for the examination of bubble swarms or for the Euler–Lagrange or Euler–Euler modelling of disperse systems. The examination of single bubbles can be done with many different perspectives. There are small bubbles with an almost spherical shape that have straight rising trajectories; there are big bubbles that rise on a helical path, while at the same time changing their shape periodically. Bubbles can be examined in quiescent liquid or under shear flow conditions, and the surrounding liquid can be pure or it can be contaminated. Due to this huge variety of aspects and in spite of many years of research, the behaviour of single gas bubbles in liquids is still not fully understood.

It is long known that small gas bubbles rising in a quiescent liquid often do not reach the rising velocity, predicted for bubbles with a perfect mobile interface. Instead, they may behave like solid particles, featuring an immobile interface (cf. Clift, Grace & Weber 1978). This is particularly true for bubbles in aqueous liquids. A common explanation for this phenomenon is the presence of trace amounts of surface-active substances in the liquid. These contaminants are adsorbed on the gas–liquid interface and are convected to the downstream cap of the bubble, where they accumulate. This

† Email address for correspondence: p.ehrhard@bci.tu-dortmund.de

https://doi.org/10.1017/S0022112009993077 Published online by Cambridge University Press

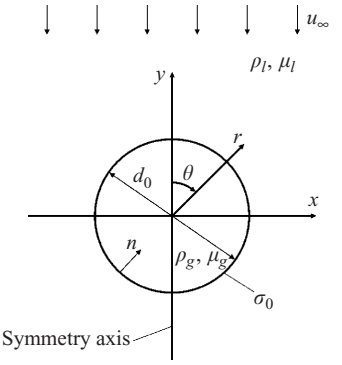


FIGURE 1. Problem sketch for a spherical bubble.

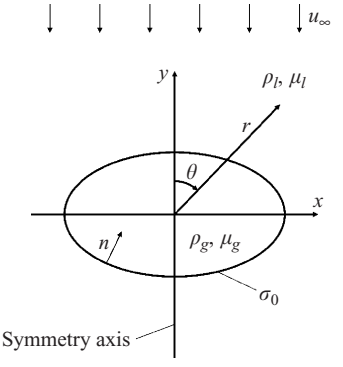


FIGURE 2. Problem sketch for an ellipsoidal bubble.

leads to a non-constant contaminant concentration along the interface, which in turn causes a non-constant surface tension. Surface tension gradients now result in shear stresses, usually directed to the upstream cap of the bubble. If we neglect, for sake of simple arguments, small shear stresses from the gas, the conditions on the gas–liquid interface, thus, change from zero shear stress to a finite shear stress (cf. Frumkin & Levich 1947). This effect is usually termed solutal Marangoni effect. Throughout this article, we use the word *contaminant* for substances that have an effect on surface tension. Even though in literature the word *surfactant* is sometimes used as synonym, in our understanding surfactants are substances, specifically designed to strongly lower surface tension.

In a first attempt to model this Marangoni effect the so-called stagnant cap model has been developed (cf. Savic 1953). Firstly, it divides the bubble surface into an upstream cap, which is supposed to be free from adsorbed contaminant and, hence, is characterized by vanishing shear stress. Secondly, a downstream cap is introduced, where the Maragoni stresses are high enough so that the relative velocity on the bubble surface vanishes and the no-slip condition holds. In the model, the size of this stagnant cap is controlled by the stagnant cap angle θ_{sc}, which is the angle at the boundary between the mobile and the immobile region of the bubble. The bubble fixed coordinate system may be found in figures 1 and 2. The limiting cases are $\theta_{sc} \to \pi$ for the shear-free bubble and $\theta_{sc} \to 0$ for the solid bubble.

https://doi.org/10.1017/S0022112009993077 Published online by Cambridge University Press

Even though the stagnant cap model is a one-parameter model, the full physical problem appears to be influenced by as many as seven parameters (cf. Cuenot, Magnaudet & Spennato 1997). Several studies in literature have attempted to verify the stagnant cap model, applying different degrees of simplification to the full physical problem. Often authors decouple the transport of the contaminant on the interface from that in the bulk. Furthermore, commonly the contaminant transport on the interface is simplified by neglecting one of the contributions: convection, diffusion, adsorption or desorption. The following publications are examples from this group. Sadhal & Johnson (1983), for the creeping flow regime, derive an analytical solution for the bubble drag as function of the stagnant cap angle. Palaparthi, Papageorgiou & Maldarelli (2006) numerically examine the influence of the bulk concentration, including bulk diffusivity as well as adsorption/desorption kinetics. Harper (1974) theoretically examines the formation of stagnant caps in surfactant solutions, including the diffusion boundary layer. Cuenot *et al.* (1997) include all contaminant transport contributions, and even couple the interface transport to the bulk transport. In their numerical study, however, they neglect bubble deformation. Hence, they obtain results on the influence of contaminations on a spherical bubble. A similar study, including bubble deformation, is made by McLaughlin (1996). Wang, Papageorgiou & Maldarelli (1999) address the influence of high bulk concentration on spherical bubbles. They engage the creeping flow limit and, therefore, also have to find a solution for the concentration field within the bulk. In a study on surfactant influence on the skin friction of bubbles, Li (2006) assumes an insoluble contaminant. Hence, he neglects adsorption and desorption, and the mass of surfactant on the interface remains constant.

The numerical methods applied to gas–liquid interfaces can be divided into two categories. Most of the above-mentioned studies use a fixed or slightly deformable computational grid, with the gas–liquid interface on one of the boundaries of the computational domain (e.g. McLaughlin 1996; Cuenot *et al.* 1997; Li 2006; Palaparthi *et al.* 2006). The contaminant transport is then computed on the two-dimensional mesh at the boundary, representing the bubble surface. This approach, though straight forward to encode, puts certain limitations on the deformation of the bubble. A different approach are immersed boundary methods (cf. Peskin 2002) or diffuse interface methods (cf. Anderson & McFadden 1998). These methods are capable of handling large deformations or even breakup of bubbles. The most notable derivatives of these approaches are the volume-of-fluid (VOF) or the level set method. Examples of applications are Renardy, Renardy & Cristini (2002), James & Lowengrub (2004), Drumright-Clark & Renardy (2004) or Xu *et al.* (2006).

In this work we apply numerical simulations to compute the distribution of a contaminant on the surface of a deformable gas bubble. Hence, we model the full contaminant transport on the gas–liquid interface, including adsorption and desorption processes, all in the frame of an immersed boundary formulation in conjunction with a modified level set method. The initially clean and stationary bubble is exposed to the contaminated liquid, which in turn, via contaminant adsorption/desorption, leads to reduced surface tension on the bubble surface. The temporal evolution of both the rising velocity and the surface contaminant concentration are computed. All these results are examined for varied physical and chemical parameters.

The article is organized as follows: following this introduction, the physical modelling and the applied assumptions and simplifications are explained in § 2, followed by some theoretical considerations on the contaminant properties. A detailed

https://doi.org/10.1017/S0022112009993077 Published online by Cambridge University Press

description of the numerical method is given in § 3. Results are presented and compared to available correlations and previous results in § 4.

2. Physical model

In this section we describe the physical model of a single gas bubble of density ρ_g and viscosity μ_g, rising in an infinite quiescent liquid of density ρ_l and viscosity μ_l. The surface tension of the clean gas–liquid interface is σ_0, the characteristic diameter of the bubble is that of a volume-equivalent sphere and is denoted by d_0. The terminal rising velocity of the bubble is u_∞. Figures 1 and 2 show sketches of the problem for both a spherical and an ellipsoidal bubble; the sketches include the bubble-fixed coordinate system (r, θ) as well as the corresponding Cartesian coordinates (x, y).

2.1. *Governing equations*

Both the gas and the liquid are considered incompressible. The respective flow fields are governed by the Navier–Stokes and the continuity equations. Using the immersed–boundary formulation as introduced by Peskin (2002), both flow fields can be described with a single set of equations, namely by

$$\rho(\phi)\left(\frac{\partial \boldsymbol{u}}{\partial t} + \boldsymbol{u}\cdot\nabla\boldsymbol{u}\right) = -\nabla p + \mu(\phi)\nabla^2\boldsymbol{u} + \rho(\phi)\boldsymbol{g} - \delta(\phi)(\nabla\sigma + \boldsymbol{n}\kappa\sigma), \quad (2.1a)$$

$$\nabla\cdot\boldsymbol{u} = 0. \quad (2.1b)$$

Here, $\boldsymbol{u}$ is the velocity vector field for both fluids, $\boldsymbol{n}$ is the interface normal vector, pointing into the gas, and κ is the mean curvature of the interface. Density and viscosity depend on the colour function ϕ; following the *continuum surface force model* as introduced by Brackbill, Kothe & Zemach (1992), the surface tension force is limited to the interface by a Dirac delta function $\delta(\phi)$, which is non-zero on the interface and vanishes everywhere else. The colour function and its computation will be described in detail in § 3.

If the liquid phase is contaminated, the constant bulk phase concentration being c_{bulk}, the contaminant can interact with the interface as discussed above. Typically, molecules are adsorbed on the upstream cap of the bubble. They are convected along the interface while at the same time being subject to molecular diffusion. On the downstream cap of the bubble, the contaminant accumulates and desorbs from the interface. Following Stone (1990), the concentration c on the interface is governed by

$$\frac{\partial c}{\partial t} + \boldsymbol{u}\cdot\nabla_s c = D_s\nabla_s^2 c + k_A c_{bulk}(1-X) - k_D X, \quad (2.2)$$

where D_s is the interface diffusion coefficient, k_A and k_D are the adsorption and desorption coefficients, $X = c/c_\infty$ is the interface coverage, which is the ratio of the actual concentration to the concentration at maximum monolayer packaging. ∇_s is the interface differential operator and can be calculated from $\nabla_s = (\boldsymbol{I} - \boldsymbol{n}\otimes\boldsymbol{n})\nabla$ (cf. Xu *et al.* 2006), where $\boldsymbol{I}$ is the unit tensor. The velocity field in (2.2) is the global velocity field. For the purpose of interpretation it may be split into a tangential and normal component. The tangential component then represents the purely convective transport along the interface, whereas the normal component represents the change in concentration due to stretching of the interface.

Depending on the size and structure of the contaminant molecules, they have a specific influence on surface tension. Most commonly, Langmuir's equation of state is

https://doi.org/10.1017/S0022112009993077 Published online by Cambridge University Press

used to express the dependency of the local surface tension on the local contaminant concentration (cf. Xu *et al.* 2006). Hence, we have

$$\sigma(c) = \sigma_0 + RTc_\infty \log(1 - X). \tag{2.3}$$

As mentioned before, σ_0 is the surface tension of the clean interface (i.e. at $c = 0$), R is the ideal gas constant and T is the temperature. It can be concluded from (2.3) that for a given system at given temperature, the only variable governing the dependency of the surface tension is the concentration at maximum packaging c_∞.

2.2. *Non-dimensionalization*

The non-dimensionalization of the above equations is based on the properties of the gas, i.e. we use the scales $\rho' = \rho/\rho_g$ and $\mu' = \mu/\mu_g$. Further, the coordinates are scaled by $\boldsymbol{x}' = \boldsymbol{x}/d_0$, using the bubble equivalent diameter; concentration by $c' = c/c_\infty$, using the maximum concentration; and surface tension by $\sigma' = \sigma/\sigma_0$, using the surface tension of the clean interface. Since the terminal velocity of a rising bubble is not known *a priori*, we define the scale $\boldsymbol{u}' = \boldsymbol{u}/u_0$, with $u_0 = \sqrt{gd_0}$, instead. Finally, pressure is scaled by $p' = p/\rho_g u_0^2$, using an inertial pressure scale, and time by $t' = t/(d_0/u_0)$. The resulting dimensionless Navier–Stokes and continuity equations are

$$\rho'(\phi)\left(\frac{\partial \boldsymbol{u}'}{\partial t'} + \boldsymbol{u}' \cdot \nabla \boldsymbol{u}'\right) = -\nabla p' + \frac{\mu'(\phi)}{Re}\Delta \boldsymbol{u}' - \rho'(\phi)\mathbf{e}_y - \frac{\delta(\phi)}{We}(\nabla\sigma' + \boldsymbol{n}\sigma'), \tag{2.4a}$$

$$\nabla \cdot \boldsymbol{u}' = 0. \tag{2.4b}$$

The dimensionless groups within (2.4*a*) are both a Reynolds and a Weber number, defined by $Re = u_0 d_0 \rho_g/\mu_g$ and $We = u_0^2 d_0 \rho_g/\sigma_0$.

The transport equation for the contaminant in dimensionless form is

$$\frac{\partial c'}{\partial t'} + \boldsymbol{u}' \cdot \nabla_s c' = \frac{1}{Pe}\nabla_s^2 c' + k'_A(1 - c') - k'_D c' \tag{2.5}$$

with the Péclet number $Pe = u_0 d_0/D_s$ and the dimensionless adsorption and desorption coefficients $k'_A = k_A c_{bulk} d_0/(c_\infty u_0)$ and $k'_D = k_D d_0/(c_\infty u_0)$.

The equation of state for the surface tension reads

$$\sigma'(c') = 1 + E \log(1 - c'), \tag{2.6}$$

with $E = RTc_\infty/\sigma_0$. E is a measure for the strength of a contaminant and is often called *surface elasticity*.

2.3. *Characterization of contaminations*

The contamination of gas–liquid interfaces appears to be a broad subject. It ranges from contaminants that have almost no effect on surface tension, even at high concentration, to contaminants that have a strong effect, even at a very low concentration. For any given contaminant, five unknowns are encountered, namely the surface diffusion coefficient D_s, the adsorption coefficient k_A, the desorption coefficient k_D, the bulk phase concentration c_{bulk} and the concentration of the fully covered interface c_∞. Since it is hardly possible to examine the influence of all these parameters, we shall limit our field of parameters by the following considerations.

The rising velocity of gas bubbles with a size of $\sim 10^{-3}$ m is $\sim 10^{-1}$ m s^{-1}. Typical diffusion coefficients are $\sim 10^{-10}$ m^2 s^{-1} or even smaller. This gives a Péclet number of $Pe \sim 10^6$, which clearly implies that diffusive transport can be neglected against

https://doi.org/10.1017/S0022112009993077 Published online by Cambridge University Press

convection. Given such strong convection in the bulk, the bubble is always in contact with fresh liquid of concentration c_{bulk}. Therefore, it appears reasonable to assume that the bulk phase concentration c_{bulk} is constant, even close to the interface. As the estimate of the Péclet number is valid likewise for the transport on the interface, we can also neglect the diffusion on the interface.

The adsorption/desorption process can be represented as an equilibrium reaction between contaminant molecules in the bulk phase S_{bulk}, free adsorption places X_{ads} and adsorbed contaminant molecules S_{ads}. Hence, we have

$$S_{bulk} + X_{ads} \rightleftharpoons S_{ads}. \tag{2.7}$$

The kinetic parameters are the adsorption and desorption coefficients k'_A and k'_D. Three cases can be discerned:

(*a*) The bulk phase is almost pure and $c_{bulk} \simeq 0$, or the contaminant is highly soluble in the liquid and k_A is small. In this case, we have $k'_A \ll k'_D$. The equilibrium is shifted to the left-hand side of (2.7). Hence, the interface remains almost clean and the surface tension is close to that of the ideal gas–liquid interface everywhere.

(*b*) The bulk phase is heavily contaminated or the contaminant is almost insoluble in the liquid, so that $k'_A \gg k'_D$ results. The equilibrium is shifted to the right-hand side of (2.7) and the interface is completely loaded with contaminant molecules. The surface tension now is close to that of the fully covered interface. Even though this surface tension is different from that of the clean interface, it is still constant everywhere.

Hence, both of these cases are of little interest when the Marangoni effect is the focus. This leaves us with the third case, namely

(*c*) adsorption and desorption are of the same order, with $k'_A \sim k'_D$.

Furthermore, if mass transport on the interface is dominated by convection, meaning that adsorption and desorption are comparatively slow, the bubble surface remains almost clean. This is because only marginal amounts of contaminant reach the interface. Hence, the surface tension is that of the clean gas–liquid interface everywhere. If, on the other hand, adsorption/desorption dominate over convection, the interface is in perfect equilibrium with the bulk. Again, the surface concentration is almost constant, as is surface tension. In all these cases no appreciable Marangoni effects can be expected. This limits the field of interest to cases where convection is of the same order as adsorption/desorption. The dimensionless terminal velocity of a solid sphere of 1mm diameter and the density of air, rising in water, turns out to be approximately equal to unity. Hence, we choose $k'_A = k'_D = 1$ for the bubble of 1mm diameter as reference. The dimensionless adsorption and desorption coefficients of spheres of different size, can then be calculated assuming that the physics of contamination remain unchanged, i.e. the dimensional properties k_A and k_D remain constant.

3. Numerical method

In the context of immersed boundary methods, a colour function ϕ is necessary to mark the spatial distribution of each phase; it is usually defined as

$$\phi(\boldsymbol{x}, t) = \begin{cases} 1 \text{ in phase 1, here the gas phase,} \\ 0 < \phi < 1 \text{ on the interface,} \\ 0 \text{ in phase 2, here the liquid phase.} \end{cases} \tag{3.1}$$

https://doi.org/10.1017/S0022112009993077 Published online by Cambridge University Press

Based on this definition, the fluid properties can be expressed by

$$\rho(\phi) = \rho_2 + \phi(\rho_1 - \rho_2), \tag{3.2a}$$

$$\mu(\phi) = \mu_2 + \phi(\mu_1 - \mu_2). \tag{3.2b}$$

The colour function is commonly handled by either the VOF method or by the level set method. The VOF method interprets the colour function as volume fraction of the liquid phase. The colour function is transported by the flow field. Since the liquid volume fraction distribution has a steep jump at the interface, interface properties such as normal or tangential vectors, or curvature, have to be reconstructed from the phase distribution (cf. Hirt & Nichols 1981).

Level set methods, on the other hand, traditionally define a level set function as a signed distance function. This means that the function value is always the shortest distance to the interface, with a positive sign in one phase and a negative sign in the other phase. Since the distance of a certain point to the interface changes in time, the level set function needs to be reinitialized at regular time intervals. The colour function can then be calculated from the level set function using a Heaviside function. The advantage of this approach is that the level set function is smooth and continuously differentiable at the interface. Normal or tangential vectors, as well as curvature, can be calculated directly without reconstruction. The major drawback of level set methods is their non-conservative nature, since the distance to the interface is a non-conservative quantity; the sum of all distances is usually not constant. Therefore, measures have to be taken to ensure mass conservation. This can be done by coupling the level set method to other methods resulting in hybrid methods like the coupled level set VOF method (cf. Sussman & Puckett 1998) or the particle level set method (cf. Enright *et al.* 2002). These hybrid methods ensure mass conservation by additional intermediate steps. This, of course, is computationally expensive and also takes away most of the original simplicity of the method.

Olsson & Kreiss (2005) propose a modified version of the level set method, which uses only a single intermediate step, and at the same time achieves mass conservation by combining the advantages of both the VOF and the level set method. Their method will be sketched in the following section.

3.1. *Transport of the colour function*

Instead of using the common distance function as level set function and calculating the colour function therefrom, Olsson & Kreiss (2005) define the level set function as the colour function ϕ in (3.1). The gas–liquid interface now is located at $\phi = 0.5$. The colour function, as usual, is transported by the flow field, based on

$$\frac{\partial \phi}{\partial t} + \boldsymbol{u} \cdot \nabla \phi = 0. \tag{3.3}$$

This level set function is now conservative, since $V_1 \simeq \int \phi \, \mathrm{d}V$ represents the volume of the phase with $\phi = 1$, which is conserved, i.e. $V_1 = \text{constant}$. This approach is almost identical to the VOF methods and ensures mass conservation. To avoid an interface reconstruction, the steep gradient of the colour function is smoothed over a distance of 2ε normal to the interface, with ε depending on the spatial mesh resolution Δx according to

$$\varepsilon = \frac{1}{2}(\Delta x)^{1-m}. \tag{3.4}$$

Here, m is a stability factor, which is set to $m = 0.1$ in accordance with Olsson & Kreiss (2005). Due to the smoothing, the modified level set function still is continuously

https://doi.org/10.1017/S0022112009993077 Published online by Cambridge University Press

differentiable, so that the interface normal vector, the curvature and the delta function can still be calculated directly from the level set function, like in the original version (cf. Sussman 1994). Hence, we have

$$\boldsymbol{n} = \left.\frac{\nabla\phi}{|\nabla\phi|}\right|_{\phi=0.5}, \tag{3.5a}$$

$$\kappa = -\nabla\cdot\boldsymbol{n}, \tag{3.5b}$$

$$\delta(\phi) = \|\nabla\phi\|. \tag{3.5c}$$

During the temporal evolution, numerical diffusion changes the width of the smoothed transition region at the interface. Higher mesh resolution or more sophisticated transport schemes reduce this error only to a certain degree. To accurately track the phase distribution, and also for the correct implementation of the surface forces, it appears important to ensure a constant width of the interface. Hence, an intermediate step is necessary to bring the smoothed transition region back to its desired width. For this purpose an artificial compression equation is engaged. It is solved to steady state during each time step and has the form

$$\frac{\partial\phi}{\partial\tau} + \nabla\cdot\boldsymbol{f}(\phi) = \varepsilon\Delta\phi. \tag{3.6}$$

The compression time variable τ is artificial and has nothing to do with time t or t'. The compression vector field $\boldsymbol{f}$ is chosen such that ϕ is convected normal to the interface, where $0<\phi<1$ holds. Hence, $\boldsymbol{f}$ is calculated from

$$\boldsymbol{f}(\phi) = \phi(1-\phi)\boldsymbol{n}_0.$$

The normal vector is only calculated once before the compression step, so that $\boldsymbol{n}_0 = \boldsymbol{n}(\tau=0)$. Thereby, the interface position is kept constant during the compression step. A compression step with pure convection would bring the transition region to a thickness of zero, which is numerically not desirable. Convection, therefore, is opposed by a defined amount of diffusion in (3.6), to ensure a smooth transition of ϕ across the interface. The diffusion coefficient is set to ε as defined in (3.4). This results in the desired width of the transition region of 2ε. The time step $\Delta\tau$ for solving (3.6) is set according to the Courant–Friedrichs–Lewi (CFL) criterion, i.e.

$$\Delta\tau = \frac{1}{2}(\Delta x)^{1+m}. \tag{3.7}$$

A spherical bubble of radius R, with its centre located at $\boldsymbol{x}_c$ can be initialized by

$$\phi(\boldsymbol{x}) = \left[1+\exp\left(\frac{|\boldsymbol{x}-\boldsymbol{x}_c|-R}{\varepsilon}\right)\right]^{-1}, \tag{3.8}$$

which is a steady-state solution of (3.6).

3.2. *Transport scheme for contaminant transport*

To incorporate a surface transport equation for the contaminant in the framework of the immersed boundary method, the two-dimensional equation (2.5) has to be transformed into a full three-dimensional transport equation, where all transport processes are limited to the interface only. This is done in the style of the continuum surface force model of Brackbill *et al.* (1992). By multiplying (2.5) with the delta function $\delta(\phi)$ and replacing $\delta(\phi)c' = c^*$, we obtain the *continuum surface transport*

https://doi.org/10.1017/S0022112009993077 Published online by Cambridge University Press

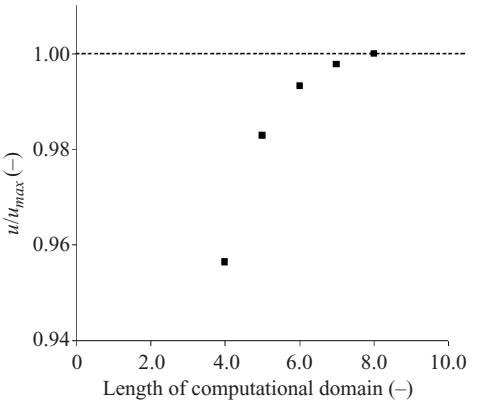


FIGURE 3. Effect of the length of the computational domain.

equation

$$\frac{\partial c^*}{\partial t} + \boldsymbol{u} \cdot \nabla c^* = \frac{1}{Pe}\nabla^2 c^* + k'_A(\delta(\phi) - c^*) - k'_D c^*. \tag{3.9}$$

The resulting continuum contaminant concentration c^* is zero everywhere but on the interface, where it has a peak of width 2ε, in perfect agreement with the smoothing width of the colour function. The normal integral of the peak represents the local concentration. If the interface concentration reaches the maximum packaging, the shape of the peak becomes identical to the delta function: $c' = 1 \Rightarrow c^* = \delta(\phi)$. Generally, the peak of c^* would disperse quickly during the computations due to numerical errors. To overcome this, an artificial compression step similar to the level set compression is applied to the contaminant concentration field. Here, it is necessary to compress the surface concentration field from both sides. At the same time, the smoothness is ensured by opposing the convective transport by a defined amount of diffusion. However, the diffusion in this case must be anisotropic and act only in normal direction. This ensures that the angular contaminant distribution is not altered during this compression step. The resulting compression transport equation is

$$\frac{\partial c^*}{\partial \tau} + \boldsymbol{h} \cdot \nabla c^* = \epsilon(\boldsymbol{n}_0 \otimes \boldsymbol{n}_0)\nabla^2 c^*, \tag{3.10}$$

with the compression vector field

$$\boldsymbol{h} = (2\phi - 1)\boldsymbol{n}_0.$$

3.3. *Computational settings*

The modified level set method and the continuum surface transport model are implemented into the open source computational fluid dynamics (CFD) code *OpenFOAM*. To minimize the size of the computational domain, the coordinate system is fixed to the bubble's centre of gravity. The upstream velocity boundary condition and the acceleration of the local reference frame are adjusted such that the bubble is kept in the centre of the computational domain. All calculations in this work are two-dimensional and axissymmetric. Careful testing during initial studies shows that a computational domain size of 6×2.5 bubble diameters appears sufficient to properly represent the flow around the free rising bubble. In figures 3 and 4 the effect of a variation of both length and width of the computational domain is shown. The obtained terminal rising velocity is plotted in dimensionless form u/u_∞ as function of

https://doi.org/10.1017/S0022112009993077 Published online by Cambridge University Press

		Water	Air
Density	ρ (kg m^{-3})	1000	1.0×10^{-3}
Viscosity	μ (Pas)	1.3	1.6×10^{-5}
Surface tension	σ_0 (Nm^{-1})	0.073	

TABLE 1. Material properties.

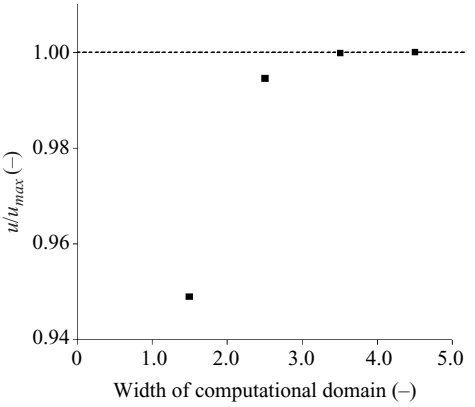


FIGURE 4. Effect of the width of the computational domain.

both length and width of the computational domain. We find that the above choice of 6×2.5 represents a reasonable compromise, with an error of the terminal rising velocity of less than 0.7 %. The computational mesh consists of square grid cells of uniform size. The optimum grid resolution was found to be $\Delta x = 0.02$, with mesh refinement resulting in no significant changes of the results. The material properties for the chosen air–water system are given in table 1.

4. Results

In the following section, firstly, a validation of the continuum surface transport model is presented. Secondly, the rising of air bubbles in water is computed for different surface elasticities. The resulting rising velocities are compared to existing correlations in literature. The terminal contaminant mass on the interface is examined. Next, the adsorption and desorption coefficients are varied, while keeping their ratio constant. Thirdly, the terminal contaminant distribution on the interface is examined. Some theoretical considerations are presented for the creeping flow limit and for moderate Reynolds numbers. The simulation results are carefully tested against these considerations.

4.1. *Validation of continuum surface transport model*

Reference information on contaminant concentration on bubble surfaces is scarce. This limits the validation of the present model to cases where an analytical solution can be inferred. As a first test, a bubble resting in a liquid of equal density, i.e. $\rho_g = \rho_l$, is computed. Initially, the bubble surface is perfectly clean. Without buoyancy, the bubble does not move, so that transport due to adsorption/desorption is not disturbed by convective transport. The temporal evolution of the concentration can, therefore, be compared to an analytical solution of (2.5), obtained for vanishing velocity and

https://doi.org/10.1017/S0022112009993077 Published online by Cambridge University Press

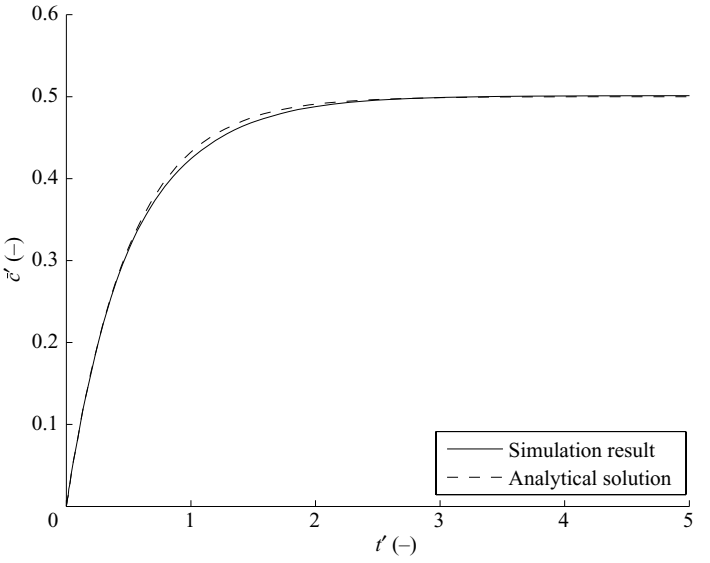


FIGURE 5. Validation of the continuum surface transport model.

vanishing surface diffusion, namely

$$c' = \frac{k'_A}{k'_A + k'_D}\left(1 - \exp\left[-(k'_A + k'_D)t'\right]\right). \tag{4.1}$$

This analytical solution has the dependence $c' = c'(t)$, meaning that a homogeneous contaminant distribution on the surface is obtained, developing exponentially towards a steady-state solution for $t \to \infty$. The numerical simulation results in the form of the surface-averaged contaminant concentration $\bar{c}'$ are compared in figure 5 to the analytical solution. The match between simulation result and the analytical solution is almost perfect. Furthermore, it can be recognized that the total contaminant mass is perfectly conserved and, likewise in the simulation, the contaminant is homogeneously distributed on the surface.

4.2. *Surface elasticity*

As discussed in § 2, the properties of the contaminant are chosen as $k'_A = k'_D = 1$ for the bubble of 1 mm diameter. This leaves the surface elasticity E in (2.6) as the only parameter. Simulations are carried out for surface elasticities in the range $0 \leqslant E \leqslant 0.04$, and for bubble diameters in the range $0.6\,\text{mm} \leqslant d_0 \leqslant 2.5\,\text{mm}$. The resulting terminal velocities for the clean bubble ($E = 0$) and for different surface elasticities are presented in figure 6. The diagram is supplemented by three correlations from literature: (i) for ideal (clean) spherical bubbles (cf. Mei, Klausner & Lawrence 1994, dash-dotted line), (ii) for ideal (clean) ellipsoidal bubbles (cf. Tomiyama *et al.* 1998, continuous line) and (iii) for spherical solid particles (cf. Schiller & Naumann 1933, dashed line). It can be recognized that the terminal rising velocity for a clean bubble (●) closely follows the prediction for the ideal spherical bubble up to a bubble diameter of 1 mm. For larger diameter, deformation affects the drag and the bubble rises slower than predicted. Eventually, for increasing d_0, the data may approach the predicted velocity of the ideal ellipsoidal bubble. If a contaminant is present, and the surface elasticity is small, $E = 0.005$, the rising behaviour of small bubbles $d_0 < 1\,\text{mm}$ appears completely different. These bubbles have a terminal rising velocity,

https://doi.org/10.1017/S0022112009993077 Published online by Cambridge University Press

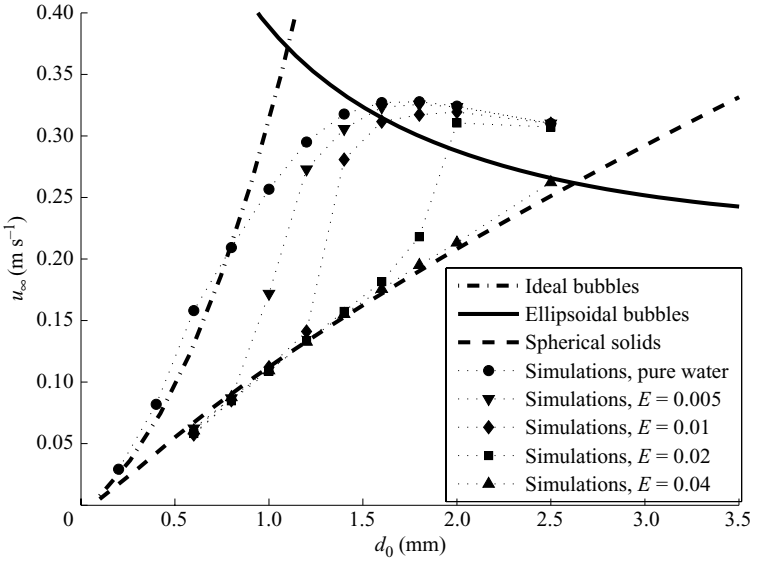


FIGURE 6. Terminal bubble velocity for varied surface elasticity.

which is identical to that of spherical solid particles. However, for increasing bubble size, these bubbles rise faster than the respective solid particles, until for $d_0 > 1.5\,\mathrm{mm}$ their rising velocity increases further and approaches that of the clean bubble. Hence, with increasing diameter, around $d_0 \simeq 1\,\mathrm{mm}$ we see a transition from a rising similar to spherical solid particles to a rising similar to clean bubbles. If the surface elasticity E is increased, this transition is shifted to larger bubble diameters, namely to $d_0 \simeq 1.5\,\mathrm{mm}$ for $E = 0.01$, and to $d_0 \simeq 1.8\,\mathrm{mm}$ for $E = 0.02$. For a surface elasticity of $E = 0.04$, even a bubble of 2.5 mm diameter rises as slow as a solid particle of comparable size.

Figure 7 depicts the dependency of the bubble terminal velocity on the surface elasticity, for the example of a bubble of 1 mm diameter. It is obvious that the bubble is immediately affected as soon as a small amount of the contaminant is present. The transition range, over which the bubble assumes the (lower) rising velocity of a solid particle, is narrow, stretching to $\Delta E \simeq 0.0075$ only. Furthermore, bubbles of different diameters all show analogous behaviour.

With these observations in mind, we now focus on the amount of contaminant, present on the interface. Figure 8 shows the mean terminal interface concentration $\bar{c}'$ as function of the bubble diameter for different surface elasticities. The mean concentration for the 'clean' bubble is obtained for $E = 0$, meaning that the contaminant transport is included in the simulation but the contaminant does not have an influence on surface tension. From this simulation it is possible to compute the total contaminant mass on the interface for the 'clean' bubble for comparison. The 'clean' bubble with $E = 0$, at all diameters, has the least amount of contaminant on the surface and, hence, the mean concentration is lowest. For all other cases with $E \neq 0$, the mean concentration is close to that of the 'clean' bubble if that bubble rises similarly fast as a clean bubble. In contrast, if at $E \neq 0$ the bubble rises similarly slow as a solid particle, we find a mean concentration of $\bar{c}' \simeq 0.5$. An integrated balance of the contaminant mass on the interface in steady-state yields

$$\bar{c}'_{theo} = \frac{k'_A}{k'_A + k'_D} = \frac{1}{2}.$$

https://doi.org/10.1017/S0022112009993077 Published online by Cambridge University Press

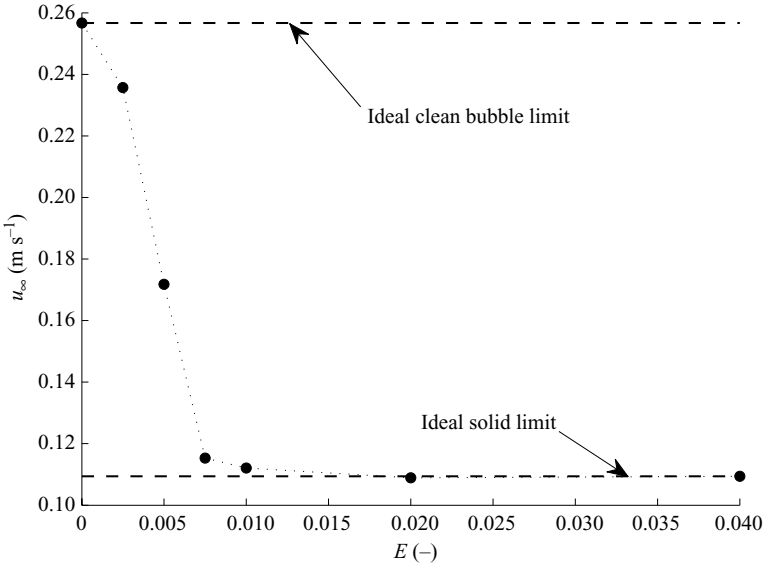


FIGURE 7. Terminal rising velocity of a 1 mm bubble for varied surface elasticity.

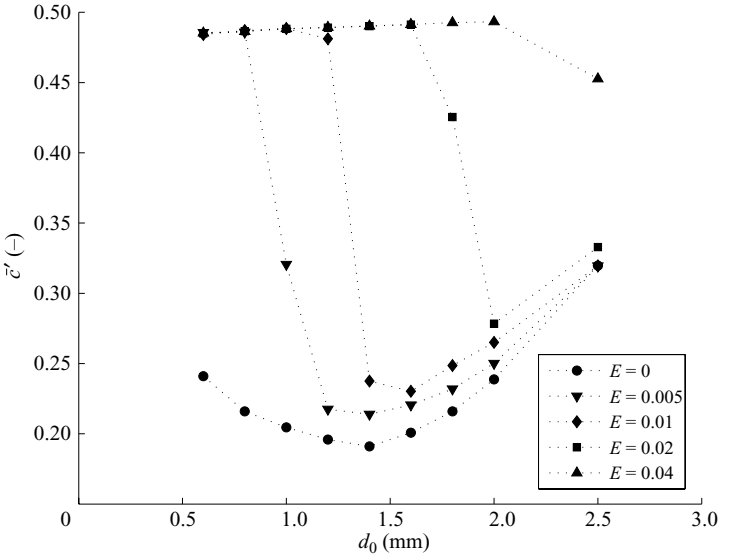


FIGURE 8. Mean terminal contaminant concentration on the interface.

From this information two things can be concluded: Firstly, any bubble that rises like a solid particle has a fully covered interface, i.e. the whole bubble surface is available for adsorption/desorption. Secondly, any bubble that does not rise like a solid particle also does not reach the equilibrium mean concentration of $\bar{c}' \simeq 0.5$. Hence, the interface is at least partially not available for adsorption/desorption. This in turn means that in some parts convection dominates, i.e. the interface is mobile.

Figures 9 and 10 show the evolution of the mean concentration and the rising velocity in time for a bubble of 1 mm diameter and three different values for the adsorption coefficient $k'_A = [0.3;\ 0.5;\ 1.0]$, while $k'_A = k'_D$ is maintained.

https://doi.org/10.1017/S0022112009993077 Published online by Cambridge University Press

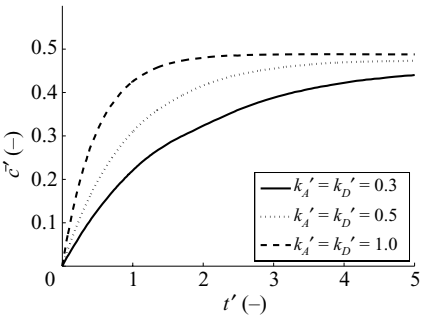


FIGURE 9. Temporal evolution of the mean concentration on a bubble of 1 mm diameter.

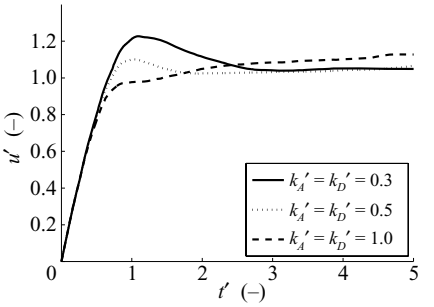


FIGURE 10. Temporal evolution of the rising velocity of a bubble of 1 mm diameter.

It is the temporal behaviour which is influenced by the adsorption/desorption coefficients: the smaller the coefficients, the slower the adsorption/desorption processes. Even though, for smaller coefficients, the steady state is reached at later times, the terminal mean concentration remains identical. As a consequence of this mean concentration history, the bubble initially may not be sufficiently retarded, accelerating to velocities higher than the terminal velocity. Only after a certain time does it slow down to the terminal velocity. This effect is stronger the smaller the coefficients. The bubble's terminal velocity, though, remains unaffected.

The observations in the above section show that very low surface elasticities are sufficient to fully retard bubbles for the given set of adsorption/desorption coefficients. For surface elasticities of a more realistic magnitude of $E \sim 10^{-1}$, the required interface concentration would be even lower. In these realistic cases, the adsorption may be slower, the desorption faster or the bulk concentration smaller. Particularly the small bulk concentration shows that even very small amounts of contaminants will suffice to fully retard a bubble.

4.3. *Distribution of contaminant on interface*

If small bubbles show the rising behaviour of solid particles, we can assume that the flow along the gas–liquid interface is retarded by Marangoni stresses until the velocity on the interface approaches zero. This implies that the Marangoni stresses should match the shear stresses, otherwise caused by the solid surface. The shear stress distribution on the surface of a spherical solid particle can be obtained either from the analytical solution for the creeping flow limit (cf. Batchelor 1967) or from numerical simulations for larger Reynolds numbers. This shear stress distribution then directly leads to the surface tension gradient profile that is necessary to achieve

https://doi.org/10.1017/S0022112009993077 Published online by Cambridge University Press

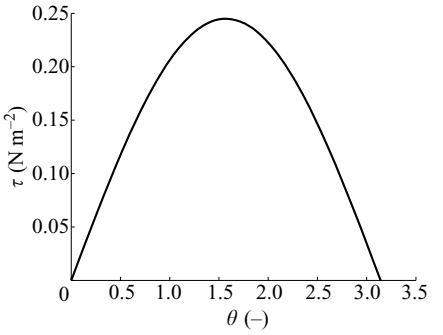


FIGURE 11. Shear stress distribution on the surface of a spherical solid particle in the creeping flow limit.

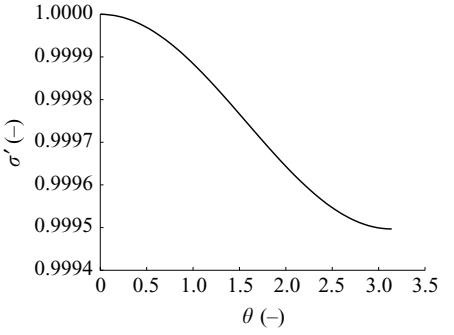


FIGURE 12. Surface tension profile that is necessary on the surface of a spherical bubble in the creeping flow limit.

a rise of the spherical bubble in accordance with the rise of a solid sphere, i.e. we obtain

$$\tau_{r,\theta} = \mu \left[r \frac{\partial}{\partial r} \left(\frac{u_\theta}{r} \right) + \frac{1}{r} \frac{\partial u_r}{\partial \theta} \right] = -\frac{1}{R} \frac{\partial \sigma}{\partial \theta}. \tag{4.2}$$

From this equation, the surface tension profile can be determined by integration. For the creeping flow limit this can be done analytically. With the boundary condition at the stagnation point $\sigma_{SP} = \sigma(\theta = 0)$, we obtain

$$\sigma(\theta) = \sigma_{\mathrm{SP}} \left[1 - \frac{3}{2} \frac{\mu_1 u_\infty}{\sigma_{\mathrm{SP}}} (1 - \cos(\theta)) \right]. \tag{4.3}$$

Determining u_∞ from Stokes law, $c_w = 24/Re$, (4.3) can be rewritten as

$$\sigma(\theta) = \sigma_{\mathrm{SP}} \left[1 - \frac{Bo}{12} (1 - \cos(\theta)) \right], \tag{4.4}$$

using the Bond number $Bo = \Delta\rho d_0^2 g/\sigma_{SP}$. The shear stress distribution on the spherical solid particle and the necessary surface tension profile on the spherical bubble surface are plotted in figures 11 and 12. From the shear stress profile in figure 11, a symmetric behaviour with the maximum shear stress at the equator ($\theta = \pi/2$) is obvious. Further, it can be concluded from figure 12 that the surface tension profile in the creeping flow limit is an odd function with respect to the bubble equator, which behaves monotonically in the complete interval $[0; \pi]$. The difference in surface

https://doi.org/10.1017/S0022112009993077 Published online by Cambridge University Press

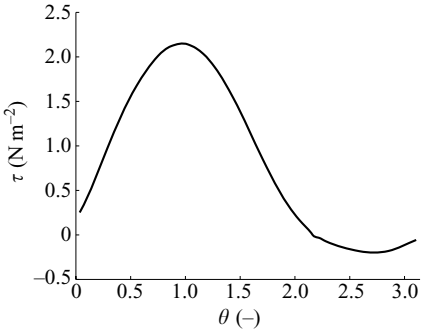


FIGURE 13. Shear stress distribution on the surface of a spherical solid particle of 1 mm diameter for $Re = 110$.

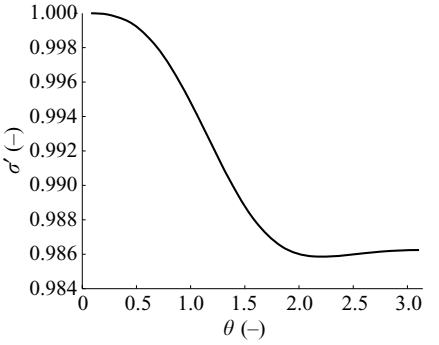


FIGURE 14. Surface tension profile that is necessary on the surface of a spherical bubble of 1 mm diameter for $Re = 110$.

tension between the upstream and the downstream stagnation point only depends on the Bond number. Since $Bo \propto d_0^2$, the difference in surface tension increases with the bubble diameter.

Finally, for a given contaminant and given surface elasticity E, the concentration profile can be calculated from the surface tension profile, using (2.3). For a bubble with $Re = 1$ and a typical surface elasticity of $E = 0.1$, the maximum surface coverage is found to be $X \simeq 5 \times 10^{-3}$. This maximum surface coverage is found at the downstream stagnation point, i.e. at $\theta = \pi$. From this we can conclude that small bubbles, which are close to the creeping flow limit, are extremely sensitive to the presence of contaminants. Even the smallest amount of contaminant changes their rising behaviour to that of a solid particle.

For larger spherical solid particles, the creeping flow limit does not hold and numerical simulations have to be applied to determine the shear stress distribution on the surface. The flow around such particles at moderate Reynolds numbers $Re < 150$ is still axissymmetric and is computed by a standard CFD package. Figure 13 shows the shear stress distribution from our numerical simulation of the flow around a particle of 1 mm diameter. The Reynolds number is $Re = 110$, the materials properties are chosen according to table 1. Figure 14 shows the corresponding surface tension profile, which again is calculated using (4.2). Comparing these profiles to that of the creeping–flow limit (cf. figures 11 and 12), the maximum shear stress can now be found upstream of the equator at $\theta \simeq 1$. Further, along the meridian the shear stress decreases below zero at $\theta \simeq 2.1$, which is the location of the flow separation line. The region with

https://doi.org/10.1017/S0022112009993077 Published online by Cambridge University Press

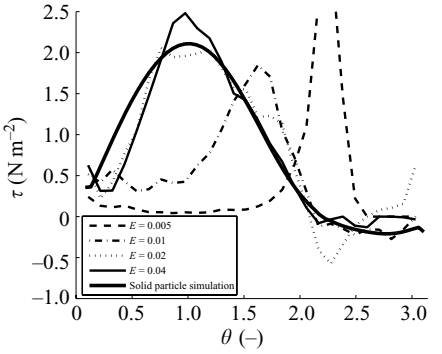


FIGURE 15. Shear stress distribution on the surface of a bubble of 1 mm diameter.

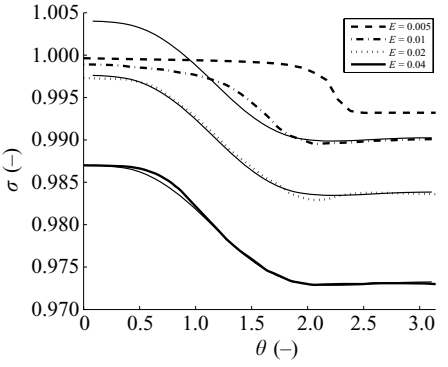


FIGURE 16. Surface tension profile, on the surface of a bubble of 1 mm diameter.

negative shear stress downstream of the separation line ($2.1 \leqslant \theta \leqslant \pi$) is caused by recirculation. Consequently, the necessary surface tension profile in figure 14 is also modified. The inflection point is now upstream of the equator at $\theta \simeq 1$ and surface tension is approximately constant downstream of the separation line.

The above observations will now be compared to results from numerical simulations with varying contaminant parameters. The bubble is now allowed to deform, though the deformation in all cases remains small, i.e. for a bubble of 1 mm diameter height/width $\leqslant 0.89$. Figure 16 shows the surface tension profiles for a bubble of 1 mm diameter and different values of the surface elasticity E. The surface tension profile from figure 14 is also included for comparison, shifted by the appropriate integration constant σ_{SP}. Three cases can be discerned:

(*a*) On bubbles that are not or only partially retarded ($E = 0.005$), surface tension is only weakly affected, it is $\sigma \simeq \sigma_0$ on the upstream cap and σ is almost constant downstream of $\theta \simeq 2.3$ The peak value of the shear stress at $\theta \simeq 2.3$ is $\tau \simeq 3.25\,\mathrm{N\ m^{-2}}$ (cf. figure 15).

(*b*) The fully retarded bubbles ($E = 0.02$, $E = 0.04$) show a surface tension profile, exactly as predicted by the above considerations. It can be concluded that fully retarded bubbles exhibit a surface tension profile such that the surface shear stress distribution is equal to that of solid particles.

(*c*) At first sight, the remaining case with a surface elasticity $E = 0.01$ appears to be a completely retarded bubble (see figure 7). Upon scrutinization, both the shear stress distribution and the surface tension profile strongly deviate from the predictions

https://doi.org/10.1017/S0022112009993077 Published online by Cambridge University Press

above. Comparing the shear stress distribution to the predicted distribution (cf. figure 15) shows that the theoretically required shear stress profile is not matched. Instead, the shear stress maximum is located further downstream than required and on the upstream cap the shear stress is almost zero. Also, on the upstream cap, surface tension is only weakly affected. Downstream of the equator, surface tension decreases and eventually reaches a constant value at $\theta \simeq 2$. The difference in surface tension between the upstream and downstream stagnation point is significantly smaller than required.

Calculating the viscous drag force of this bubble gives 80 % of the value obtained for the solid particle. As the viscous drag in the third case makes up 51 % of the overall drag, the drag coefficient reduces by 10 %, and the terminal velocity increases by 5 %. Careful examination of figure 6 indicates that this bubble actually is not fully retarded. Its rising velocity is only close to that of the solid particle. Hence, we conclude that partially contaminated interfaces generate Marangoni stresses that are strong enough to gradually slow down the bubble, but a fully covered interface is necessary to completely slow down the bubble to the rising velocity of a solid sphere.

5. Conclusions

In the present work, the influence of small amounts of contaminations in the liquid on the rising behaviour of gas bubbles is examined, with the focus on Marangoni stresses generated by adsorption/desorption of the contaminant on the bubble surface. The examinations are limited to convection-dominated transport in the bulk and on the bubble's surface. Preliminary considerations show that the adsorption and desorption kinetics should be of the same order, and moreover should be of comparable order as convective transport. The influence of the surface elasticity is examined numerically. The free interface is represented by a modified level set method. A continuum surface transport model is presented, which includes the transport of contaminant on the gas–liquid interface into the framework of an immersed boundary formulation.

The terminal rising velocities of air bubbles in water are computed. In the absence of a contaminant, the terminal rising velocities show perfect agreement to correlations in literature on ideal clean bubbles. In the presence of a contaminant, the bubble rising velocity eventually decreases to the rising velocity of a solid particle. It is shown that the surface of such bubbles is fully covered with contaminant. The contaminant distribution is such that the surface tension profile generates Marangoni stresses that match the shear stress distribution on the surface of a solid particle of identical properties.

Further investigations will focus on the determination of the set of contamination parameters that are necessary to slow down a given bubble to the rising velocity of a corresponding solid particle. This set of parameters is given by the adsorption coefficient, the desorption coefficient, and the surface elasticity. This will make it possible to classify contaminations, based on their influence on rising bubbles.

This article is dedicated to Professor S. H. Davis, on the occasion of his 70th birthday. We would like to express our thanks to the Deutsche Forschungsgemeinschaft (DFG) for funding this research project. Furthermore, we gratefully acknowledge collaboration within this project with Professor F. Peters from the Ruhr-University in Bochum.

https://doi.org/10.1017/S0022112009993077 Published online by Cambridge University Press

REFERENCES

Anderson, D. M. & McFadden, G. B. 1998 Diffusive-interface methods in fluid mechanics. *Annu. Rev. Fluid Mech.* **30**, 139–168.

Batchelor, G. K. 1967 *An Introduction to Fluid Dynamics*. Cambridge University Press.

Brackbill, J. U., Kothe, D. B. & Zemach, C. 1992 A continuum method for modelling surface tension. *J. Comput. Phys.* **100**, 335–354.

Clift, R., Grace, J. R. & Weber, M. E. 1978 *Bubbles, Drops, and Particles*. Academic Press.

Cuenot, B., Magnaudet, J. & Spennato, B. 1997 The effects of slightly soluble surfactants on the flow around a spherical bubble. *J. Fluid Mech.* **339**, 25–53.

Drumright-Clark, M. A. & Renardy, Y. 2004 The effect of insoluble surfactant at dilute concentration on drop breakup under shear with inertia. *Phys. Fluids* **16**, 14–21.

Enright, D., Fedkiw, R., Ferizger, J. & Mitchel, I. 2002 A hybrid particle level set method for improved interface capturing. *J. Comput. Phys.* **183**, 83–116.

Frumkin, A. & Levich, V. G. 1947 On surfactants and interfacial motion. *Zhurnal Fizicheskoi Khimii* **21**, 1183–1208.

Harper, J. F. 1974 On spherical bubbles rising steadily in dilute surfactant solutions. *Q. J. Mech. Appl. Math.* **17**, 87–100.

Hirt, C. W & Nichols, B. D. 1981 Volume of fluid (VOF) method for the dynamics of free boundaries. *J. Comput. Phys.* **39**, 201–225.

James, A. J. & Lowengrub, J. 2004 A surfactant-conserving volume-of-fluid method for interfacial flows with insoluble surfactant. *J. Comput. Phys.* **201**, 685–722.

Li, J. 2006 The effect of an insoluble surfactant on the skin friction of a bubble. *Eur. J. Mech.* B/*Fluids* **25**, 59–73.

McLaughlin, J. B. 1996 Numerical simulation of bubble motion in water. *J. Colloid Interface Sci.* **184**, 614–625.

Mei, R., Klausner, J. F. & Lawrence, C. J. 1994 A note on the history force on a spherical bubble at finite Reynolds number. *Phys. Fluids* **6**, 418–420.

Olsson, E. & Kreiss, G. 2005 A conservative level set method for two phase flow. *J. Comput. Phys.* **210**, 225–246.

Palaparthi, R., Papageorgiou, D. T. & Maldarelli, C. 2006 Theory and experiments on the stagnant cap regime in the motion of spherical surfactant-laden bubbles. *J. Fluid Mech.* **559**, 1–44.

Peskin, C. S. 2002 The immersed boundary method. *Acta Numer.* **11**, 479–517.

Renardy, Y. Y., Renardy, M. & Cristini, V. 2002 A new volume-of-fluid formulation for surfactants and simulations of drop deformation under shear at low viscosity ratio. *Eur. J. Mech.* B/*Fluids* **21**, 49–59.

Sadhal, S. S. & Johnson, R. E. 1983 Stokes flow past bubbles and drops partially coated with thin films. Part 1. Stagnant cap of surfactant film – exact solution. *J. Fluid Mech.* **129**, 237.

Savic, P. 1953 Circulation and distortion of liquid drops falling through a viscous medium. *Natl Res. Counc. Can. Div. Mech. Engng Rep.* **MT–22**, 1–35.

Schiller, L. & Naumann, A. Z. 1933 Über die grundlegenden Berechnungen bei der Schwerkraftaufbereitung. *Zeitung VDI* **77**, 318–320.

Stone, H. A. 1990 A simple derivation of the time-dependent convective-diffusion equation for surfactant transport along a deforming interface. *Phys. Fluids* A **2**, 111–112.

Sussman, M. 1994 A level set approach for computing solutions to incompressible two-phase flow. *J. Comput. Phys.* **114**, 149–159.

Sussman, M. & Puckett, E. G. 2000 A coupled level set and volume of fluid method for computing 3D and axissymmetric incompressible two-phase flows. *J. Comput. Phys.* **162**, 301–337.

Tomiyama, A., Kataoka, I., Zun, I. & Sakaguchi, T. 1998 Drag coefficients of single bubbles under normal and micro gravity conditions. *Japan Soc. Mech. Engnng Intl J. Ser.* B **41**, 472–479.

Wang, Y., Papageorgiou, D. T. & Maldarelli, C. 1999 Increased mobility of a surfactant–retarded bubble at high bulk concentrations. *J. Fluid Mech.* **390**, 251–270.

Xu, J.-J., Li, Z., Lowengrub, J. & Zhao, H. 2006 A level-set method for interfacial flows with surfactant. *J. Comput. Phys.* **212**, 590–616.

https://doi.org/10.1017/S0022112009993077 Published online by Cambridge University Press